Self-Engaging Spined Gripper with Dynamic Penetration and Release for Steep Jumps

Jessica S. Lee*, Mark Plecnik*, Je-han Yang, and Ronald S. Fearing

***Abstract*— Due to high impact forces and low duty cycles, monopedal jumping robots are particularly susceptible to failure from a slipping foot. Spines provide a solution to reduce slip, but there has been little research on how to effectively engage them into a surface with a dynamic jumping robot. Previous robots utilizing spines operate in different regimes of surface approach speed and cycle time. For a penetrable substrate, spines must be directed into the surface at suitable holding angles, then extracted before the foot leaves the ground. We accomplished this by designing a gripper mechanism for the robot Salto that pushes in angled spines along their length and is kinematically constrained to engage/disengage with leg crouch/extension. The resulting mechanism introduces no new actuators, enables jumping on penetrable inclines up to 60°, and enables static adhesion to hold 7.5 times the robot's weight from a ceiling.**

I. Introduction

Jumping robots are useful due to their ability to navigate obstacles many times their body height. They can be used for search and rescue missions in collapsed buildings or monitoring areas that are at risk. Small robots have many applications due to the fact that they are easily transportable and able to access small spaces. However, there are many challenges associated with these robots because their size limits the amount of onboard processing, motors or batteries that can be used. This paper focuses on a gripper design for traction and adhesion capabilities for Salto, a small robot capable of repeated, high-powered jumps [1], [2] (Fig. 1). Adhesion is a prerequisite for perching, useful for surveillance and rationing energy. Higher traction enables the robot to jump at both steep and shallow angles without encountering an irrecoverable slip, allowing navigation over tall obstacles as well as under low overhangs.

II. Previous Work

Bio-inspired passive mechanisms and smart mechanical systems have been used in recent years to significantly improve robot performance. One such strategy is the addition of spines, which has been implemented in terrestrial running [3][4], climbing [5][6][7][8][9][10], and perching [11][12][13]. Spines work on dirty and rough surfaces, do not require additional onboard processing or power, and can last many cycles. Previous implementations capable of engaging and disengaging from a surface are shown in Fig. 2.

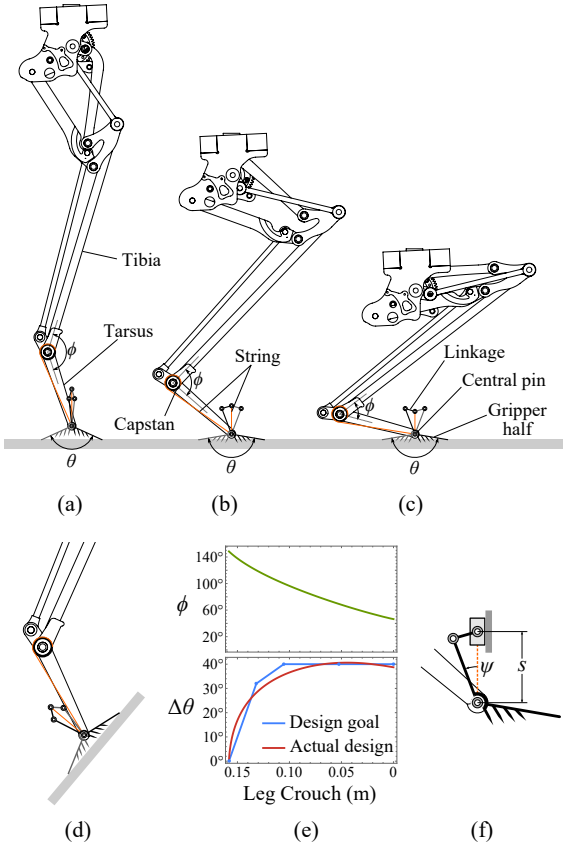

Fig. 1. Schematic of a Salto leg mechanism modified with a kinematically coordinated gripper. (a) The gripper is disengaged when the leg is extended, (b) then engages and (c) remains engaged for various stages of crouch. (d) Despite coupling engagement to leg crouch, gripper orientation remains decoupled to be defined by incline angle. (e) The kinematic task involves coordinating the tibia-tarsus angle ϕ to a gripper open/close angle θ. (f) This coordination is accomplished by modelling one half of the gripper as a slider-crank function generator.

Climbing robots quasi-statically engage vertical surfaces with cycle times comparable to a slow walk. On the other extreme, flying robots equipped with perching mechanisms dynamically encounter surfaces, but are not designed to engage/disengage on a locomotive timescale. Little research on spine engagement has been performed in between these extremes. An outlier to these two groups is DROP, a climbing robot that utilizes multiples spines on a wheel to dynamically engage a surface and climb at high speeds [14].

This material is based upon work supported by the National Science Foundation under IGERT Grant No. DGE-0903711, NSF Grant No. DGE-1106400 and CMMI-1636302 and by the Army Research Laboratory under the Micro Autonomous Systems and Technology Collaborative Technology Alliance.

Jessica S. Lee and Je-han Yang are with the Department of Mechanical Engineering. Mark Plecnik and Ronald S. Fearing are with the Electrical Engineering and Computer Sciences, University of California, Berkeley, CA 94720 USA jessica-lee@berkeley.edu, mplecnik@berkeley.edu

*These authors contributed equally to this work.

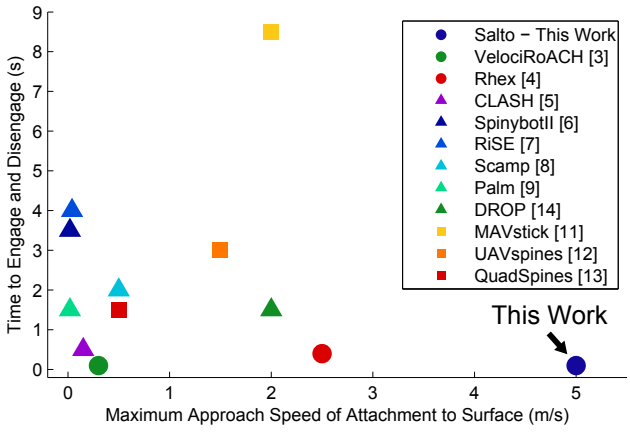

Fig. 2. Comparison of previous applications of spines according to their approach speed to a surface and time to engage and disengage. Values were estimated if not immediately available. Terrestrial robots are circles, climbing robots are triangles, and perching mechanisms for flying robots are squares.

The goal of this work is to improve traction for an agile jumping robot which operates on stance timescales shorter than perching robots but dynamically approaches surfaces unlike climbing robots, see Fig. 2. Previous research of spines on terrestrial robots include VelociRoACH, which obtained higher speeds and walkable incline angles through traction [3], and RHex, who used spines to traverse mesh [4]. The only other jumping robot to utilize spines for traction is the flea-inspired robot of [15], but spines were only used during takeoff, since the robot could not make repeated jumps. Using spines to penetrate a surface has been explored for climbing robots [16], but could also be useful for terrestrial traction. This is the first spined gripper kinematically coupled to engage and disengage on a jumping robot.

III. Gripper Design

Designing a self-engaging gripper mechanism involved (A) kinematically coordinating leg configuration to gripper engagement, (B) calculating spine mounting, and (C) prototyping, as described in the following.

A. Kinematic Coordination

We aim to design a gripper for Salto that is kinematically constrained to engage when the leg crouches and disengage when the leg extends. In particular, we aim for the gripper to move to an engaged configuration as the robot begins to crouch, then to remain engaged for all other leg configurations, see Fig. 1(a)–(c). Moreover, gripper orientation must be decoupled from engagement motion, allowing the contact angle with a surface to define this additional degree-of-freedom, Fig. 1(d). To attain these goals, we use the relative angle between the tibia and tarsus links, labelled as ϕ in Fig. 1, as a generator of motion at the tarsus. A string that connects to the tibia-tarsus joint routes to the topmost pin of the linkage where it acts as a linear actuator, pulling the top pin toward the central pin and opening two gripper halves. The opening action engages spines into the surface. As the leg uncrouches this process is reversed; the string relaxes and a rubber band pulls the gripper halves together, disengaging the spines and pushing the top pin away from the central pin.

The linkage and tarsus form a two degree-of-freedom five-bar. The joints connecting each gripper half to the tarsus are made coincident, decoupling gripper orientation from its open/close motion. The remaining design challenge is to choose linkage dimensions such that the open/close motion is coordinated with leg extension. The tibia-tarsus angle ϕ is a function of leg extension which is proportional to string travel transmitting linear motion to the top joint of the linkage. Angle ϕ is plotted in Fig. 1(e) along with the desired coordination between leg extension and gripper abduction angle $\Delta\theta$. To achieve this coordination, one half of the linkage may be considered as a slider-crank function generator, Fig. 1(f), coordinating input string travel s to an output angle ψ that measures the orientation of a gripper half. Following the procedure of [17], we designed the link proportions shown in Fig. 1(f) that produce the desired dwell function with $\Delta\theta$ shown in Fig. 1(e).

B. Directed Spine Velocities

Strategies for engaging spines include catching asperities [6], pinching material [18], and penetrating the substrate [16]. As our focus is the latter, we require that the opening motion of the gripper results in spines piercing the substrate. To accomplish this, spines were mounted onto the gripper so that they point along their velocity vectors at the moment of entering the substrate. In this section, we introduce a model for calculating spine mounting. First, we show how to compute mounting angle for the choice of spine tip location. Second, we compute spine tip locations for the choice of penetration angle, resulting in a family of curves. Plotting these curves serves as a useful tool when designing spine tip entry points.

1) Calculating Mounting Angles: The motion of a gripper half relative to the substrate was modelled as a link with ends constrained to orthogonal lines: one line being the horizontal contact surface and the other lying coincident to vertical travel of the central pin (labelled in Figs. 1(c) and 3(a)). It is well known that a point attached to this link (referred to as the *coupler*) traces an ellipse. Taking the horizontal axis as the substrate boundary, its intersection with a trace ellipse and the tangency angle with the ellipse may be computed and transformed to coordinates local to the coupler frame.

As shown in Fig. 3(a), the length of a gripper half is l and its configuration is parameterized by a single variable b, the height of the central pin above the surface. For a specified spine tip point c, we desire to compute the angle κ at which to mount the spine. A point c in the moving coupler frame M has global frame coordinates C,

$$C = ib + \frac{c}{l}\left(\sqrt{l^2 - b^2} - ib\right), \tag{1}$$

where real and imaginary components contain (x, y) coordinates. Point C contacts the surface when $C = \bar{C}$ (overbar

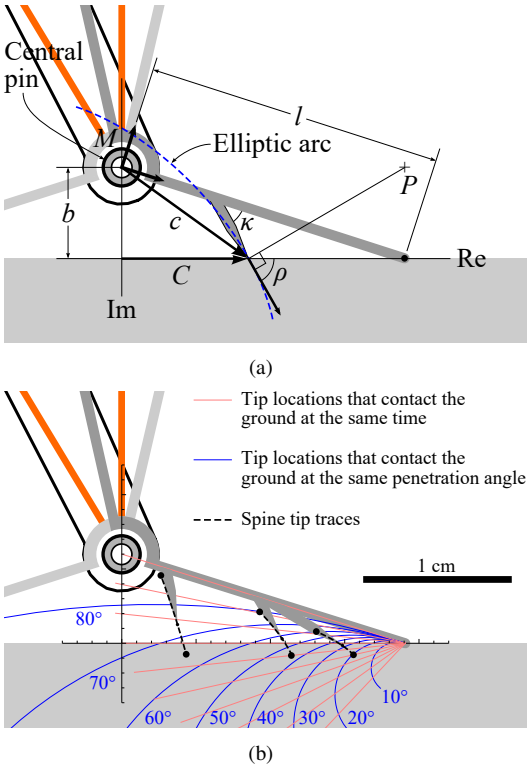

Fig. 3. (a) Relative motion between a gripper half and the substrate was modelled as a link with one end as the contact point sliding horizontally and the other end as the central pin travelling vertically. (b) Analyzing the space of elliptic traces afforded by this model discovers a family of constant contact angle arcs from which we choose spine tip locations and angle spines accordingly.

denotes conjugate), at which the configuration variable b evaluates to

$$b = \frac{il\,(c-\bar{c})}{2\sqrt{(l-c)\,(l-\bar{c})}}. \tag{2}$$

To compute the angle ρ of the velocity vector at contact, substitute (2) into the derivative of (1), take the argument, and apply appropriate offsets to obtain,

$$\rho = -\arg\left(1+\frac{c}{l}\left(\frac{c-\bar{c}}{c+\bar{c}-2l}-1\right)\right)-\frac{\pi}{2}. \tag{3}$$

The angle κ at which the spine mounts to the gripper half follows the trigonometry of Fig. 3(a).

2) Calculating Spine Tip Locations: As an inverse problem, it is also useful to find points c that produce a desired penetration angle ρ. A point c contacts the surface with velocity vector angled at ρ if the line that passes through global point C and coupler pole P is angled $\frac{\pi}{2}-\rho$ from horizontal i.e. said line is perpendicular to the velocity vector of angle ρ. Therefore, we combine the following three equations,

pole of coupler: $\quad P = \sqrt{l^2-b^2}+ib$

line through P at angle $\frac{\pi}{2}-\rho$: $\quad \dfrac{C-P}{\bar{C}-\bar{P}} = \dfrac{1+i\tan\left(\frac{\pi}{2}-\rho\right)}{1-i\tan\left(\frac{\pi}{2}-\rho\right)}$

line along real axis: $\quad C-\bar{C}=0$

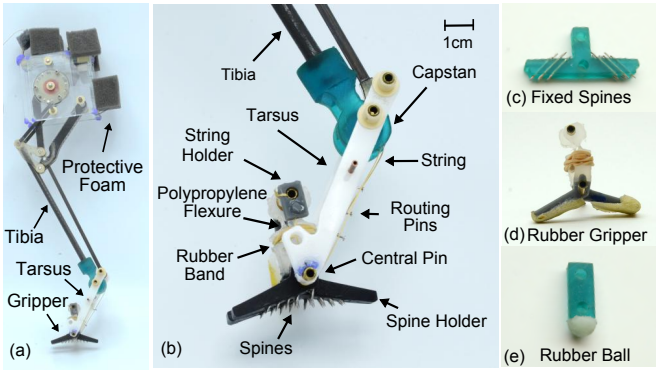

Fig. 4. (a) Salto Body with gripper attachment. (b) Gripper with spines attached to the robot. (c) End effector with spines held fixed at 43° from horizontal. (d) Gripper with rubber attached to the bottom instead of spines. (e) 3D printed end effector with a rubber hemisphere attached (referred to as a *rubber ball*).

to formulate an expression for C,

$$C = \sqrt{l^2-b^2}-b\tan\rho, \tag{4}$$

which may be transformed into coordinates of local frame M,

$$c = c_\rho(b) = l - \frac{bl\tan\rho}{\sqrt{l^2-b^2}-ib}. \tag{5}$$

Note that for a given ρ, a curve of points c parameterized by b exists, motivating the notation $c = c_\rho(b)$. The family of arcs $c_\rho(b)$ may be plotted alongside lines radiating from the sliding contact as a design tool for relating spine tip contact timing and penetration angle, see Fig. 3(b). A diversity of penetration angles were selected in order to engage a variety of substrates. Those angles, depicted in Fig. 3(b), are 74.0°, 57.4°, and 32.7°.

C. Manufacturing

The gripper is made up of three subsystems: the capstan, the string subsystem, and the linkage. The capstan is 3D printed and attached to the base of the tibia (Fig. 4(b)). The string subsystem consists of the pins, string tightener, and an aramid fiber string. There are two large pins: the central pin located at the bottom of the tarsus that the linkage is free to rotate around, and the topmost pin of the linkage that gets pulled toward the central pin when the linkage is actuated. Smaller routing pins are inserted into the tarsus to guide the string from the capstan to the topmost pin. Routing pins ensure the string does not interfere with the swing motion of the linkage through the tarsus and direct string tension so as to return the linkage to a centered orientation when it is not in ground contact. The string originates from the capstan and terminates into string holders that sit on either side of the topmost pin. These string holders have a cylinder that the end of the string twists around, thereby removing any slack in the string.

There are three separate linkage halves for force balancing. The top of a linkage half consists of a milled out polypropylene piece with a hole to connect to the topmost pin and a flexure that acts as a joint. The polypropylene also acts as a

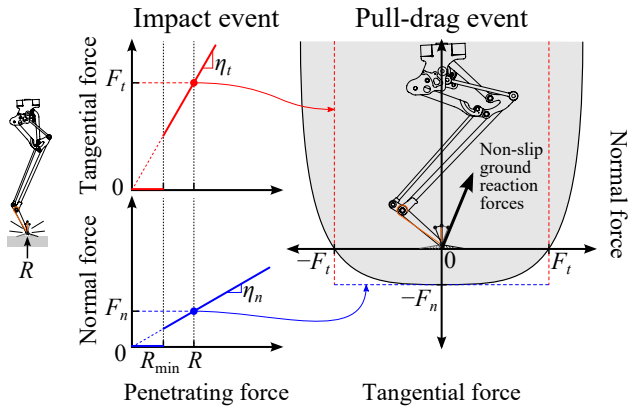

Fig. 5. At the time of impact, spines penetrate into a substrate, affording a space of non-slip ground reaction forces during a pull-drag event in the future. The coefficients of engagement, η_t and η_n, model maximal non-slip tangential F_t and adhesive F_n forces as proportional to the previously occurring impact R. This model is only valid if a threshold penetrating force R_{min} is surpassed.

return spring by pushing the top pin away from the central pin until a rubber band takes over. The polypropylene is glued to a 3D printed piece with holes to direct the exact angle of the spines. To control the length of the spines during assembly, a 3D printed fixture was used to accurately position spine tips to certain heights. After sliding the spines through their mounting holes and positioning them with the fixture, they are glued in place.

A first spined gripper was constructed with spines angled according to the model in Fig. 3(b), where there is a combination of steep spines for penetrating a surface [16] and shallow spines to engage along the surface for traction [6]. A second spined gripper specializes in adhesion forces and has steeper and longer spines for better penetration. Several other foot designs were constructed to serve as controls that were tested against (Fig. 4(c)-(e)), including an end effector with fixed spines, a gripper covered in rubber, and an end effector with a rubber hemisphere at the end (referred to as a *rubber ball*).

IV. Coefficient of Engagement

An obvious candidate for measuring ground contact engagement is the coefficient of friction. However, this quantity does not describe the adhesive loads which are readily apparent of penetrated spines. Furthermore, the ground reaction force we aim to describe has a history dependent aspect to it: a spine embedded at the time of an impact defines the range of ground reaction forces possible during a normal or tangential loading event in the future, see Fig. 5.

Therefore, in order to characterize the performance of a penetrating gripper, we propose the *coefficient of engagement* (η_n and η_t), defined by the ratio of a maximal statically generated normal load F_n or tangential load F_t to the impact force R which enabled that load in the first place. Furthermore, we require R to be greater than the minimum impact R_{min} required for penetration.

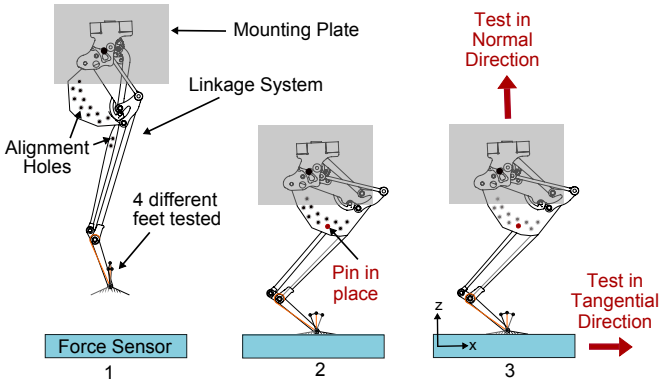

Fig. 6. Static testing procedure to find CoE. (1) The leg is lowered onto the force sensor. (2) The leg is lowered to a certain amount of crouch and pinned in place. (3) The leg is slowly pulled in the normal or tangential direction.

Unlike friction, our definition relaxes the requirement for a normal force to be present in order to measure a tangential force. Instead, tangential and normal reaction forces are proportional to a previous impact force, allowing tangential loading in the absence of normal force or adhesion in the absence of a tangential load. The assumption of proportionality is based off previous work by [16], as well as handbook guidelines on fastener extraction [19].

In the case that impact and tangential loading do proceed simultaneously, then coefficient of engagement in the tangential direction degenerates into coefficient of friction. This is the case with dynamic loading events such as the stance phase in between jumps.

V. Static Engagement

A. Methods

To experimentally determine the coefficient of engagement (CoE) for the gripper mechanism, we attached it to a Salto leg made out of Delrin. It should be noted that for all our CoE tests we used the first spined gripper, which has a larger range of spine angles. The leg contains alignment holes in two links so that when the links pass in front of each other, the leg could be constrained with a pin (Fig. 6). The holes were positioned to test the CoE's for different stages of crouch. This leg was attached to a platform that could be controlled in the vertical (z) direction and utilized spring loaded linear bearings for force control in the vertical and horizontal (x) directions. Sample material was attached to the force sensor (ATI Mini45) which was bolted onto a platform that could be controlled in the x-y plane. The test procedure is shown in Fig. 6 where the leg is lowered onto a force sensor, pinned in a certain crouched position, and pulled in the tangential or normal direction to the surface.

The spined gripper was tested against the fixed spines, a gripper covered in rubber, and a rubber ball (Fig. 4), all tested at different stages of crouch. The different materials used were cork, rigid open-celled foam, acrylic, and sandpaper to obtain a variety of penetrable and impenetrable surfaces of different asperity sizes. Each test varied the end effector type, crouch amount, and surface material and was repeated

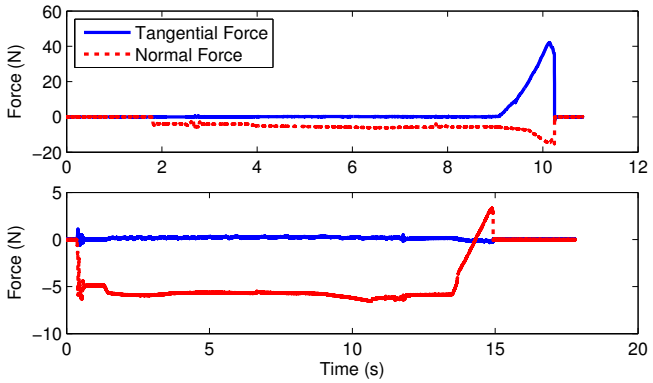

Fig. 7. Force sensor data from the static test in the tangential (top) and normal (bottom) directions. Both tests were conducted on cork at 70% crouched.

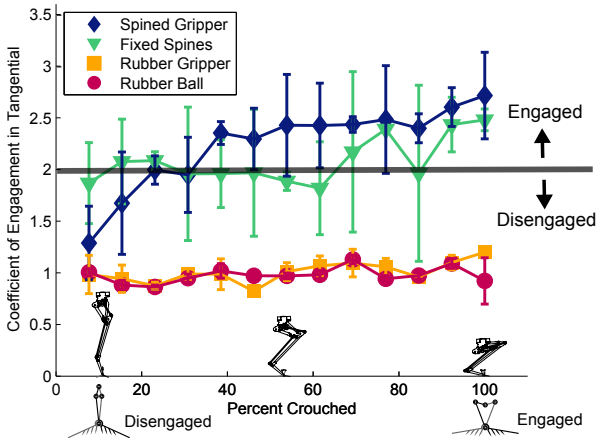

Fig. 8. Coefficient of engagements taken from static testing on cork in the tangential direction. Coefficient of engagement is plotted versus leg crouch, where to the left it is fully extended and to the right it is fully crouched. The gripper diagram on the bottom left illustrates how the gripper is disengaged when the leg is uncrouched, and the spines are not able to penetrate the surface. But on the right the gripper is engaged and the spines dig into the surface. The engaged/disengaged line highlights how the spined gripper is disengaged from the surface and has a low CoE up until it is over 30% crouched.

three times. An example set of force sensor data for a CoE test in tangential loading and adhesion can be seen in Fig. 7. CoE was calculated by taking the maximum force needed to disengage the end effector from the surface divided by the penetration force present when first engaging the end effector into the surface.

B. Results

An example set of data on cork can be seen in Fig. 8 where there were high CoE's for the spined gripper and fixed spines, but low values for the gripper with rubber and the rubber ball. Although both spined gripper and fixed spines have high values, the gripper has a method of disengaging from a material by simply uncrouching, as shown by the values when the gripper is less than 30% crouched. Since the other end effectors showed similar performance no matter the amount crouched, we were able to average the CoE values

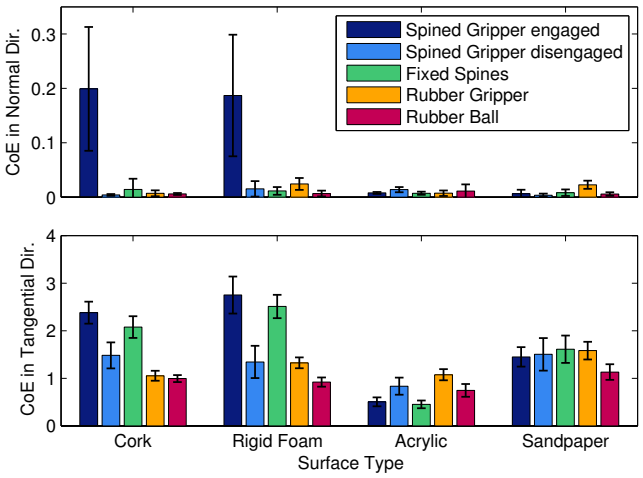

Fig. 9. Static testing for CoE in normal and tangential loading for all end effectors and surfaces after being statically engaged.

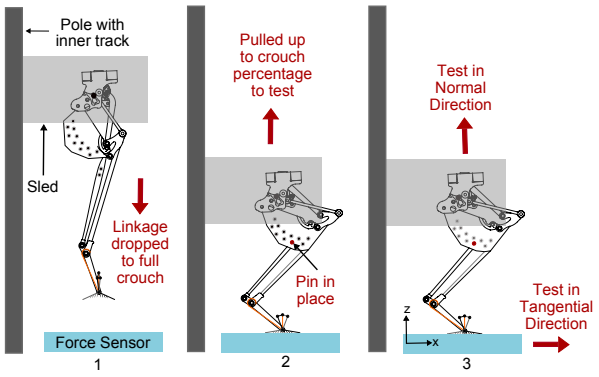

Fig. 10. Drop testing procedure for CoE. (1) Leg system is dropped from 34cm to the force sensor into a fully crouched position. (2) The sled is pulled upwards, allowing the leg to uncrouch to the specific percentage of crouch that is being tested. Then the leg is pinned in place. (3) The leg is pulled in either the normal or tangential direction.

for fixed spines, rubber gripper, and rubber ball respectively into Fig. 9. For the spined gripper we averaged the CoE depending on whether it was below 30% crouched or over. In the normal direction (Fig. 9), only the engaged spined gripper exhibited a substantial coefficient of engagement on cork and rigid foam. This indicates that while the leg is crouched, the gripper provides the robot with adhesion. Performance on impenetrable surfaces (acrylic and sandpaper) was similar for all end effectors, but in the tangential direction the rubber gripper engages the most on acrylic because it has a high amount of rubber contacting the surface. In the tangential direction, the engaged spined gripper and the fixed spines have high CoE's on the penetrable surfaces (cork and rigid foam), but when the gripper is uncrouched it can function more like a rubber ball and can disengage from a surface. The spined gripper while crouched showed a 1.4 times improvement over a simple rubber ball on cork and a 2 times improvement on rigid foam.

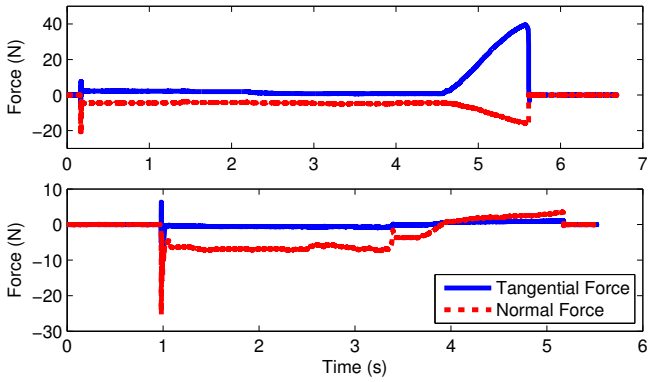

Fig. 11. Force sensor data from the dynamic engagement test in the tangential (top) and normal (bottom) directions. Both tests were conducted on cork at 70% crouched.

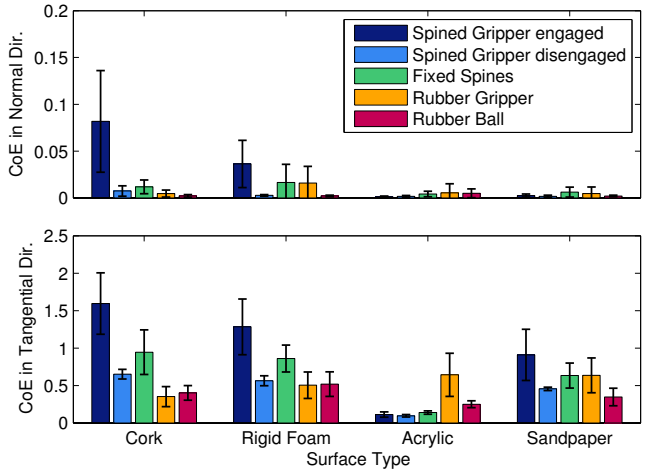

Fig. 12. Dynamic engagement testing for CoE in normal and tangential loading for all end effectors and surfaces after being dynamically engaged.

VI. Dynamic Engagement

To verify that the gripper performs in a dynamic application, we first tested its ability to dynamically engage with a surface. The leg used in the static tests was attached to a sled connected to a linear bearing in a tall pole with an inner track. The test procedure can be seen in Fig. 10. In order to make sure the leg did not bounce back up, the leg acted as an overdamped system by adding a rubber band to bias it toward being extended and increased its body mass with the sled. An example data set for the drop test in tangential and normal directions is shown in Fig. 11.

The CoE was lower for these dynamic tests due to oscillations during spine engagement. The CoE was lower for these dynamic tests due to additional oscillations during spine engagement. The crouched spined gripper increased the CoE in the tangential direction by 3 times on cork and 1.5 times on rigid foam compared to the rubber ball. Again, the CoE in the normal direction was substantial for the spined gripper on cork and rigid foam during dynamic engagement tests (Fig. 12). The fixed spines and rubber gripper were also able to develop some adhesive forces on foam. The uncrouched spined gripper was able to disengage material

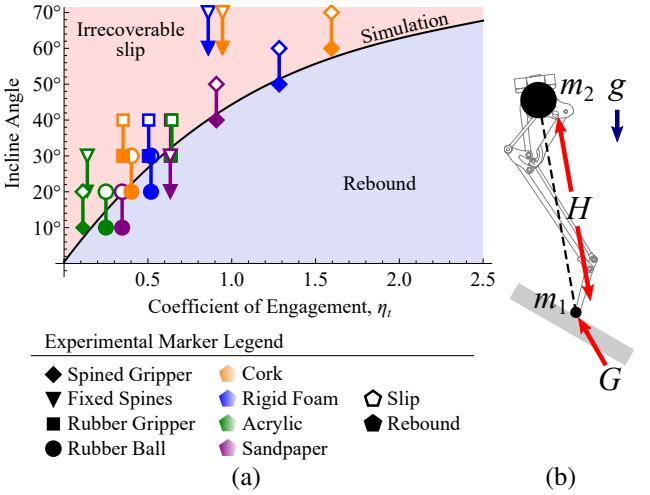

Fig. 13. (a) A comparison of the simulation and experimental results displaying the maximum incline angle on which a gripper with a certain dynamic tangential coefficient of engagement may successfully execute a rebound jump. The area under the curve represents the space of successful rebounds indicated by simulation. Plot markers indicate experimental results. Successful rebounds occurred at filled markers and irrecoverable slips occurred at open markers. (b) Free-body diagram used for dynamic simulation. Force H follows Salto's variable mechanical advantage curve presented in [2].

during dynamic engagement tests. These CoE values are used in the dynamic model from Section VII to predict how different feet should perform on a dynamic, jumping robot.

VII. Simulation of Dynamics

In order to understand coefficient of engagement from a task level, we simulated rebounds onto inclined planes to find the relationship between coefficient of engagement η_t and maximum incline angle, see Fig. 13(a). A gripper with $\eta_t = 1.0$ falling 50cm may at best rebound off a $44°$ angle, whereas $\eta_t = 2.0$ yields a $63°$ angle.

This result was computed from the two mass model shown in Fig. 13(b), where m_1 represents the robot's end effector and m_2 represents the body. The normal component of contact dependent force G includes a stiffness of 10^4 N/m and damping coefficient of 20 Ns/m. The tangential component models η_t as Coulombic friction. H is modelled from the force profile and variable mechanical advantage of Salto's leg, printed in Fig. 10 of [2], and additionally includes internal friction and damping multiplied by configuration-dependent mechanical advantage.

Equations of motion were derived through direct application of Newton's second law on the two masses. The resulting ordinary differential equations and contact conditions were formatted as an initial value problem for integration with the MATHEMATICA function *NDSolve*.

VIII. Jumping Experiments

After testing the gripper's ability to dynamically engage, we wanted to test whether it can also dynamically release from the surface. To test its ability to disengage, we constructed a free drop test where the body was hanging by a releasable string, dropping the robot by 50cm. The body

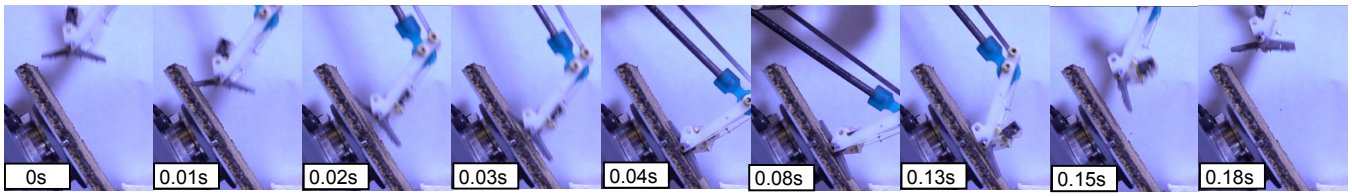

Fig. 14. Close up video stills of the spined gripper jumping off cork at 60°. At 0.01s the gripper hits the cork and starts rotating towards the surface. At 0.04s it engages the surface and starts to crouch. By 0.13s the robot has crouched down, uncrouched, and is just about to jump off the surface. At 0.18s the gripper has successfully rotated itself back to its neutral position.

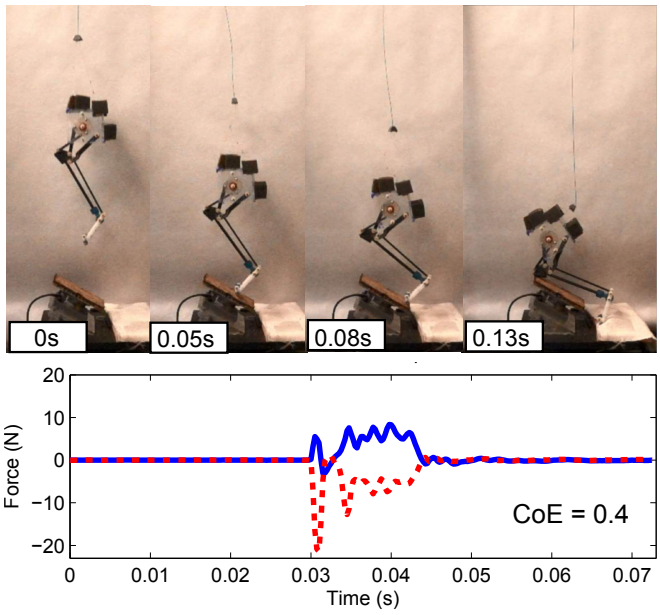

Fig. 15. Video stills of the robot with a rubber ball slipping off cork at 30° with the force sensor data underneath.

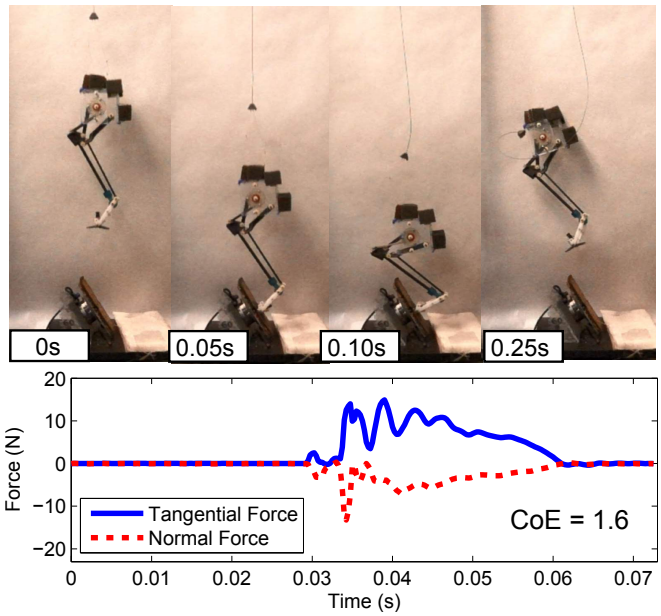

Fig. 16. Video stills of the robot with the spined gripper jumping off cork at 60° with the force sensor data underneath.

nested into a fixture at the start to ensure the same orientation every drop. The robot body was constructed with Salto's parts including its latex spring, so when the robot dropped it would crouch, energize the spring and rebound back up. This Salto skeleton weighed 80g, and we placed an additional 58g on the body to better mimic the loading of a full Salto assembly and balance out the added gripper weight to minimize angular momentum during jump. To quantify each end effectors' performance on cork, rigid foam, acrylic and sandpaper, we dropped the Salto skeleton onto fixed inclined surfaces. Video stills of the rubber ball slipping on a 30° cork surface are shown in Fig. 15 and the spined gripper rebounding on a 60° cork surface is shown in Fig. 16. A close up view of the gripper engaging the surface for a different 60° cork trial can be seen in Fig. 14.

Experimental results are plotted alongside free drop simulation results in Fig. 13. Data points mark measured dynamic CoE values versus the maximum experimental rebound angle for 16 different gripper/substrate combinations. Each maximum rebound angle is presented within a range between a lower bound (filled marker) and upper bound (open marker). Lower bounds were established by completing 3 out of 5 successful rebounds, and upper bounds were established when this did not happen. Incline angles were tested in 10° increments. Simulation details were described in Section VII.

Here fixed spines seemed to outperform the spined gripper and the dynamic simulation. Although fixed spines yielded a lower CoE than the spined gripper during the dynamic engagement tests, they were able to jump at higher inclines than expected. This is partially explained by their freely rotating end effector. This end effector was able to rotate onto steep surfaces faster than the spined gripper halves, which were slowed by string tension from the capstan mechanism. Also, steeper test angles increased the tangential component of the insertion force to nicely match the angle of the fixed spines.

IX. Adhesion Experiments

Although the static tests with the current spined gripper demonstrated the capability to perch onto penetrable substrates, preliminary experiments were conducted to test the spined gripper's ability to adhere to a ceiling. Using the design principles from Section III and knowledge obtained from our experiments, a second spined gripper was constructed that had steeper angles and longer spines to better penetrate surfaces (Fig. 17c). The gripper was attached to

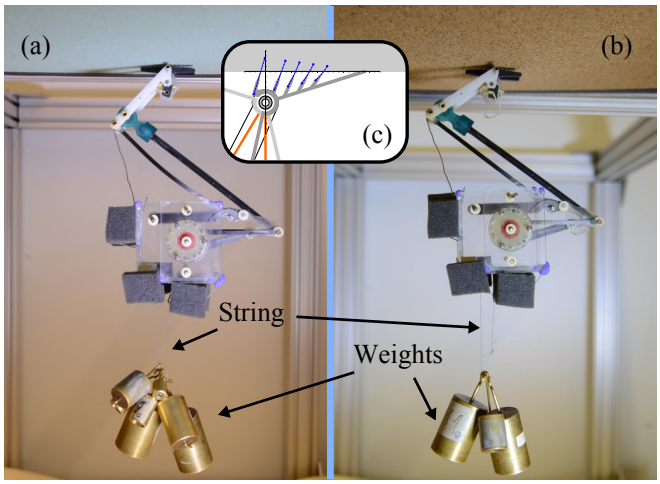

Fig. 17. Salto skeleton with spined gripper design adhered to (a) rigid foam and (b) cork with additional weight hanging from its body.

the Salto skeleton and crouched onto a ceiling of either rigid foam or cork. The leg was latched in place to keep the robot crouched. Then weights were added until either Salto fell or we reached the weight limit that puts Salto's body near breaking stress. There were eight trials performed for cork and five for rigid foam. The robot was able to carry $433 \pm 35g$ additional weight on cork and $514 \pm 79g$ on rigid foam (Fig. 17). Rigid foam reached the weight limit of $600g$ twice. The variation in weight supported was caused by surface variation and the sway of hanging weights, allowing the spines to slip out.

X. Discussion and Conclusions

In this paper we present a gripper mechanism with spines to be used on Salto, a highly dynamic robot. This is the first work to demonstrate spines on a jumping robot that can dynamically penetrate and release from a surface. Our gripper's function is dependent on its kinematic design. Energy from landing impacts is transformed through the robot's crouching motion to direct spines into penetrable surfaces at angles that match their velocity vectors. Release from a surface is allowed by coupling spine disengagement to the uncrouching motion of Salto. To measure surface engagement, the coefficient of engagement (CoE) was introduced, which describes the range of possible ground reaction forces enabled by a previously occurring impact event. Our spined gripper increased the tangential CoE by 1.4 times on cork and 2 times on rigid foam compared to the control case of a rubber ball. The additional traction enabled by this improvement allowed the robot to jump off 60° inclines on cork and rigid foam, as opposed to just 20° with a rubber ball, matching our dynamic model. Our gripper design also enables adhesive loads, allowing the robot to hold 6.3 times its body weight on cork and 7.5 times on rigid foam. This work details a new strategy for managing the ground reaction force of jumping robots, with a particularly focus on mitigating slip scenarios on penetrable surfaces.

Acknowledgment

The authors would like to thank Carlos Casarez and Justin Yim for their valuable insights and manufacturing help, and Ethan Schaler for photography. We also gratefully acknowledge the support of our funding sources. Any opinions, findings, and conclusions or recommendations expressed in this material are those of the authors and do not necessarily reflect the views of the National Science Foundation.

References

[1] D. W. Haldane, M. Plecnik, J. K. Yim, and R. S. Fearing, "Robotic vertical jumping agility via series-elastic power modulation," *Science Robotics*, vol. 1, no. 1, p. eaag2048, 2016.

[2] M. Plecnik, D. W. Haldane, J. K. Yim, and R. S. Fearing, "Design exploration and kinematic tuning of a power modulating jumping monopod," *Journal of Mechanisms and Robotics*, vol. 9, no. 1, p. 011009, 2016.

[3] J. S. Lee and R. S. Fearing, "Anisotropic collapsible leg spines for increased millirobot traction," *IEEE Int. Conf. on Robotics and Automation*, vol. 2015-June, no. June, pp. 4547–4553, 2015.

[4] J. C. Spagna, D. I. Goldman, P.-C. Lin, D. E. Koditschek, and R. J. Full, "Distributed mechanical feedback in arthropods and robots simplifies control of rapid running on challenging terrain," *Bioinspiration & Biomimetics*, vol. 2, no. 1, pp. 9–18, 2007.

[5] P. Birkmeyer, A. G. Gillies, and R. S. Fearing, "CLASH: Climbing vertical loose cloth," *IEEE Int. Conf. on Intelligent Robots and Systems*, pp. 5087–5093, 2011.

[6] A. T. Asbeck, S. Kim, M. R. Cutkosky, W. R. Provancher, and M. Lanzetta, "Scaling Hard Vertical Surfaces with Compliant Microspine Arrays," *The Int. Journal of Robotics Research*, vol. 25, no. 12, pp. 1165–1179, 2006.

[7] M. J. Spenko, G. C. Haynes, J. A. Saunders, M. R. Cutkosky, A. A. Rizzi, R. J. Full, and D. E. Koditschek, "Biologically inspired climbing with a hexapedal robot," *Journal of Field Robotics*, vol. 25, no. 4-5, pp. 223–242, 2008.

[8] M. T. Pope, C. W. Kimes, H. Jiang, E. W. Hawkes, M. A. Estrada, C. F. Kerst, W. R. Roderick, A. K. Han, D. L. Christensen, and M. R. Cutkosky, "A Multimodal Robot for Perching and Climbing on Vertical Outdoor Surfaces," *IEEE Transactions on Robotics*, vol. 33, no. 1, pp. 38–48, 2017.

[9] S. Wang, H. Jiang, and M. R. Cutkosky, "A palm for a rock climbing robot based on dense arrays of micro-spines," in *Intelligent Robots and Systems, 2016 IEEE/RSJ Int. Conf. on*. IEEE, 2016, pp. 52–59.

[10] C. Y. Lin and H. Y. Chueh, "Design and implementation of a wall-jumping robot with climbing claws," *Journal of the Chinese Institute of Engineers*, vol. 40, no. 1, pp. 45–54, 2017.

[11] M. Kovač, J. Germann, C. Hürzeler, R. Y. Siegwart, and D. Floreano, "A perching mechanism for micro aerial vehicles," *Journal of Micro-Nano Mechatronics*, vol. 5, no. 3, pp. 77–91, 2009.

[12] A. Lussier Desbiens, A. T. Asbeck, and M. R. Cutkosky, "Landing, perching and taking off from vertical surfaces," *The Int. Journal of Robotics Research*, vol. 30, no. 3, pp. 355–370, 2011.

[13] D. Mellinger, M. Shomin, and V. Kumar, "Control of Quadrotors for Robust Perching and Landing.pdf," *Int. Powered Lift Conf.*, pp. 119–126, 2010.

[14] K. Carpenter, N. Wiltsie, and A. Parness, "Rotary Microspine Rough Surface Mobility," *IEEE/ASME Transactions on Mechatronics*, vol. 21, no. 5, pp. 2378–2390, 2016.

[15] J. S. Lee, R. S. Fearing, and K.-J. Cho, "Compound foot for increased millirobot jumping ability," in *Advances in Cooperative Robotics*, 2016, pp. 71–78.

[16] W. R. Provancher, J. E. Clark, B. Geisler, and M. R. Cutkosky, "Towards Penetration-based Clawed Climbing," *Climbing and Walking Robots*, vol. 27, no. 2, pp. 961–970, 2005.

[17] M. Plecnik and J. M. McCarthy, "Five position synthesis of a slider-crank function generator," in *ASME 2011 IDETC/CIE Conf.*, Washington, D.C., August 2011.

[18] M. Plecnik and R. S. Fearing, "A study on finding finite roots for kinematic synthesis," in *ASME 2017 IDETC/CIE Conf.*, Cleveland, OH, August 2017.

[19] E. A. Avallone and T. Baumeister III, *Marks' Standard Handbook for Mechanical Engineers*, 10th ed. New York, NY: McGraw Hill, 1996.